

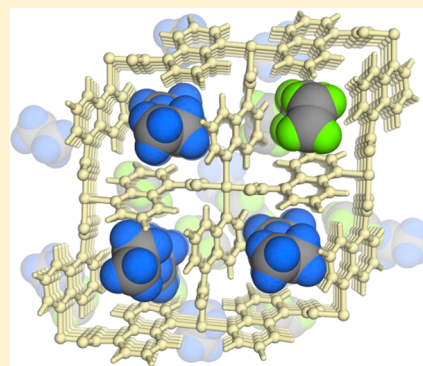
Boosting Ethane/Ethylene Separation within Isorecticular Ultramicroporous Metal–Organic Frameworks

Rui-Biao Lin,[†] Hui Wu,[‡] Libo Li,[†] Xiao-Liang Tang,[†] Zhiqiang Li,[†] Junkuo Gao,[†] Hui Cui,[†] Wei Zhou,^{*,‡} and Banglin Chen^{*,†}

[†]Department of Chemistry, University of Texas at San Antonio, One UTSA Circle, San Antonio, Texas 78249-0698, United States
[‡]NIST Center for Neutron Research, National Institute of Standards and Technology, Gaithersburg, Maryland 20899-6102, United States

Supporting Information

ABSTRACT: The separation of ethane from its analogous ethylene is of great importance in the petrochemical industry, but very challenging and energy intensive. Adsorptive separation using C₂H₆-selective porous materials can directly produce high-purity C₂H₄ in a single operation but suffers from poor selectivity. Here, we report an approach to boost the separation of C₂H₆ over C₂H₄, involving the control of pore structures in two isorecticular ultramicroporous metal–organic framework (MOF) materials with weakly polar pore surface for strengthened binding affinity toward C₂H₆ over C₂H₄. Under ambient conditions, the prototypical compound shows a very small uptake difference and selectivity for C₂H₆/C₂H₄, whereas its smaller-pore isorecticular analogue exhibits a quite large uptake ratio of 237% (60.0/25.3 cm³ cm⁻³), remarkably increasing the C₂H₆/C₂H₄ selectivity. Neutron powder diffraction studies clearly reveal that the latter material shows self-adaptive sorption behavior for C₂H₆, which enables it to continuously maintain close van der Waals contacts with C₂H₆ molecules in its optimized pore structure, thus preferentially binds C₂H₆ over C₂H₄. Gas sorption isotherms, crystallographic analyses, molecular modeling, selectivity calculation, and breakthrough experiment comprehensively demonstrate this unique MOF material as an efficient C₂H₆-selective adsorbent for C₂H₄ purification.



INTRODUCTION

Separation and purification of chemical mixtures are energy-intensive processes currently in the chemical industry that take up substantial cost. Several bulk chemical commodities involving the light olefins, such as ethylene (C₂H₄) and propylene (C₃H₆), are the cornerstone of many important manufacturing, exceeding a worldwide production of 200 million tonnes.¹ To separate ethylene from its analogous ethane of very similar molecular size and volatility, a typical industrial process highly relies on heat-driven cryogenic distillation through repeated distillation–compression cycles, which is one of the most energy-intensive technologies. The corresponding energy consumption for such separation is estimated to be about 7.3 GJ per tonne of ethylene.² Consequently, there is an urgent demand to explore alternative technologies and materials that can efficiently separate and purify these light hydrocarbons under mild conditions. It is well recognized that nonthermal separation technologies like adsorption-based or membrane-based ones can be more highly energy efficient than the cryogenic distillation technology.³

Utilizing the differences of the molecular geometry and physical properties, porous materials can exhibit differential adsorption for various components of the mixture.⁴ However, except for a few chemisorbents,⁵ conventional porous materials show poor adsorption selectivity for hydrocarbons mixture due

to the lack of recognition mechanism. As novel porous materials, metal–organic frameworks (MOFs) and/or porous coordination polymers (PCPs) have the advantage of designable structures with tunable pore sizes and diverse functionalities,⁶ that enables them to show promise for a wide variety of applications in many important areas,⁷ including olefin/paraffin separation.⁸ The core of MOF chemistry lies in their construction approach, referring to the connections of specific building blocks over multiple dimensions via coordination bonds. Introduction of functional sites into MOFs can enhance binding interaction for polar hydrocarbons, while precise control over the pore sizes can exclude larger molecules, both resulting in improved separation performance. A series of important progresses have been achieved by using MOFs as porous media in the realms of C₂H₄/C₂H₆,⁹ C₂H₂/C₂H₄,¹⁰ C₃H₆/C₃H₈,¹¹ and C₃H₄/C₃H₆ separation.¹²

For equilibrium separation via physical adsorption, the separation performance is determined by the host–guest interactions between the porous framework and the adsorbates, including dispersion and electrostatic interactions.¹³ These interactions rely on the surface properties of the adsorbent and the nature of the adsorbate molecule, such

Received: July 17, 2018

Published: September 14, 2018

as dipole moment, quadrupole moment, polarizability, and so on.¹³ For adsorbents with highly polarized or high electric field gradient surfaces (e.g., functionalized with open metal sites), the electrostatic interactions often dominate. Thus, gas molecules with high dipole and/or quadrupole moments are preferentially bound.^{13,14} In contrast, for adsorbents with inert pore surfaces (e.g., featuring aromatic or aliphatic moieties) like activated carbon, dispersion and induction interactions make major contributions, which are proportional to the polarizability of gas molecules.¹³ Consequently, given the fact that C₂H₄ shows a larger quadrupole moment (C₂H₄: 1.50 × 10⁻²⁶ esu cm², C₂H₆: 0.65 × 10⁻²⁶ esu cm²) while C₂H₆ has a larger polarizability (C₂H₄: 42.52 × 10⁻²⁵ cm³, C₂H₆: 44.7 × 10⁻²⁵ cm³),¹⁴ MOFs used for C₂H₄/C₂H₆ separation can be cataloged into C₂H₄-selective MOFs^{9a,b} and C₂H₆-selective MOFs.¹⁵ The latter is proposed to be much more efficient for related separation, as it can simplify the separating process for high-purity C₂H₄ and thus cut down the corresponding energy consumption.^{15a} The design strategies for C₂H₄-selective MOFs are relatively straightforward, that is, introducing highly polar binding centers like open metal sites or hydrogen-bonding acceptor to boost the selectivity.^{9b,16} In contrast, owing to the lack of suitable strong binding site, C₂H₆-selective MOFs usually suffer from poor selectivity. Also, the C₂H₆/C₂H₄ uptake ratios of the benchmark C₂H₆-selective MOFs are just over 1, as they show quite similar capacities for both gases,¹⁵ which limit their available capacities for ethane capture from C₂H₄/C₂H₆ mixture. A feasible strategy is to increase the efficient contact area or the quantity of interactions between C₂H₆ molecules and the host framework (forming multiple interactions), for which ultramicroporous MOFs are more favorable, but precise control on the pore chemistry is required.

By virtue of the isorecticular principle in MOF chemistry, we were able to target two isorecticular ultramicroporous MOF materials, [Cu(ina)₂] (Hina = isonicotinic acid; here termed as Cu(ina)₂) and [Cu(Qc)₂] (Qc-5-Cu-sq,¹⁷ HQc = quinoline-5-carboxylic acid; here termed as Cu(Qc)₂), to exhibit the control of pore chemistry for advancing C₂H₆/C₂H₄ selectivity. The accessible pore surface of these two MOFs mainly features aromatic rings of low polarity, enabling preferential binding of ethane over ethylene. Particularly, activated Cu(Qc)₂ exhibits a smaller pore aperture size of about 3.3 Å, facilitating possible multiple adsorbent–adsorbate interactions in confined pore space, which motivated us to check its potential for C₂H₆/C₂H₄ separations. Gas sorption studies indicate that Cu(Qc)₂ is clearly a ethane-selective adsorbent with a superior C₂H₆/C₂H₄ uptake ratio of 237% and selectivity of 3.4, which are much higher than those of its isorecticular analogue Cu(ina)₂ with a larger pore. Direct crystallography studies reveal that C₂H₆ molecules can be well accommodated by the self-adaptive framework of Cu(Qc)₂ with optimized pore structure, which can maximize the number of weak host–guest interactions and/or the corresponding close contact area. As a result, Cu(Qc)₂ can preferentially capture C₂H₆ from the C₂H₆/C₂H₄ mixture under ambient conditions, affording a superior porous adsorbent for the challenging separation of C₂H₆/C₂H₄. Molecular modeling studies and experimental breakthrough have well supported the claim.

EXPERIMENTAL SECTION

Materials and Physical Measurements. All reagents and solvents were commercially available and directly used without

further purification. Thermogravimetric analysis (TGA) was carried out under an air atmosphere from room temperature to 900 °C using a Shimadzu TGA-50 analyzer at a heating rate of 10 °C min⁻¹. Powder X-ray diffraction (PXRD) patterns were collected using a Rigaku Ultima IV diffractometer (Cu Kα) at 40 kV and 44 mA with a scan rate of 8.0° per min.

The gas sorption measurements were performed on an automatic volumetric adsorption apparatus Micromeritics ASAP 2020 surface area analyzer. Prior to the gas sorption analyses, as-synthesized samples were activated according to the literature.^{17,18} The experimental temperatures were controlled by dry ice–acetone bath (195 K), ice–water bath (273 K), water bath (298 K), and heating jacket (313 K), respectively.

Synthesis of Cu(ina)₂. Cu(ina)₂ was previously synthesized.¹⁸ A mixture of Cu(NO₃)₂·2.5H₂O (0.116 g, 0.5 mmol), Hina (0.123 g, 1.0 mmol), I₂ (0.127 g, 0.5 mmol), and water (6 mL) was placed in a Teflon-lined stainless steel vessel (12 mL) and heated at 140 °C for 72 h, and then it was cooled to room temperature at a rate of 5 °C h⁻¹. The resulting black block crystals of [Cu(ina)₂]₂·I₂ were collected and washed with water and acetone, then dried in the air (yield 0.17 g, 61%).

Synthesis of Cu(Qc)₂. Cu(Qc)₂ was previously synthesized.¹⁷ A mixture of Cu(BF₄)₂·6H₂O (0.10 g, 0.29 mmol), HQc (0.10 g, 0.58 mmol), *N,N'*-dimethylformamide (DMF, 6 mL), and EtOH (6 mL) was placed in a scintillation vial (20 mL) and heated at 105 °C for 48 h, and then it was cooled to room temperature at a rate of 6 °C h⁻¹. The resulting dark purple block crystals were collected and washed with DMF and EtOH, then dried in the air (yield 0.095 g, 68%).

Neutron Crystallography. Powder neutron diffraction data were collected using the BT-1 neutron powder diffractometer at the National Institute of Standards and Technology (NIST) Center for Neutron Research. A Ge(311) monochromator with a 75° takeoff angle, λ = 2.0787(2) Å, and in-pile collimation of 60 min of arc was used. Data were collected over the range of 3–166.3° (2θ) with a step size of 0.05°. A fully activated Cu(Qc)₂ sample was loaded in a vanadium can equipped with a capillary gas line and a packless valve. A closed-cycle He refrigerator was used for sample temperature control. The activated Cu(Qc)₂ sample was measured first at the temperature of 298 K. To probe the gas adsorption locations, C₂D₆ and C₂D₄ (note that deuterated gas was used because H has a large incoherent neutron scattering cross section and thus would introduce large background in the diffraction data) were loaded into the sample at room temperature, and diffraction data were then collected on the gas-loaded MOF samples. Different C₂D₆ loadings into Cu(Qc)₂ were realized by controlling the loading pressure.

Rietveld structural refinement was performed on the neutron diffraction data using the GSAS package.¹⁹ Due to the large number of atoms in the crystal unit cell, the ligand molecule and the gas molecule were both treated as rigid bodies during the Rietveld refinement, with the molecule orientation and center of mass freely refined. Final refinement on the positions/orientations of the rigid bodies, thermal factors, occupancies, lattice parameters, background, and profiles converged with satisfactory *R*-factors.

Crystallographic data and refinement information were summarized in Table S1. CCDC 1852578–1852581 contains the supplementary crystallographic data of [Cu(Qc)₂]₂·0.41C₂D₆, [Cu(Qc)₂]₂·0.16C₂D₄, [Cu(Qc)₂]₂·0.67C₂D₆ and [Cu(Qc)₂]₂, respectively. These data can be obtained free of charge from the Cambridge Crystallographic Data Centre via www.ccdc.cam.ac.uk/data_request/cif.

RESULTS AND DISCUSSION

Considering the pore sizes and physical properties of the pore surface, copper isonicotinate (Cu(ina)₂) was chosen as the prototype MOF.¹⁸ To introduce large organic moieties for further control over the pore chemistry, ligands with extra aromatic rings were targeted to construct isorecticular structures. Quinoline-4-carboxylic acid and quinoline-5-carboxylic acid have met such requirements. However, there is no accessible pore volume in copper quinoline-4-carboxylate,²⁰ so

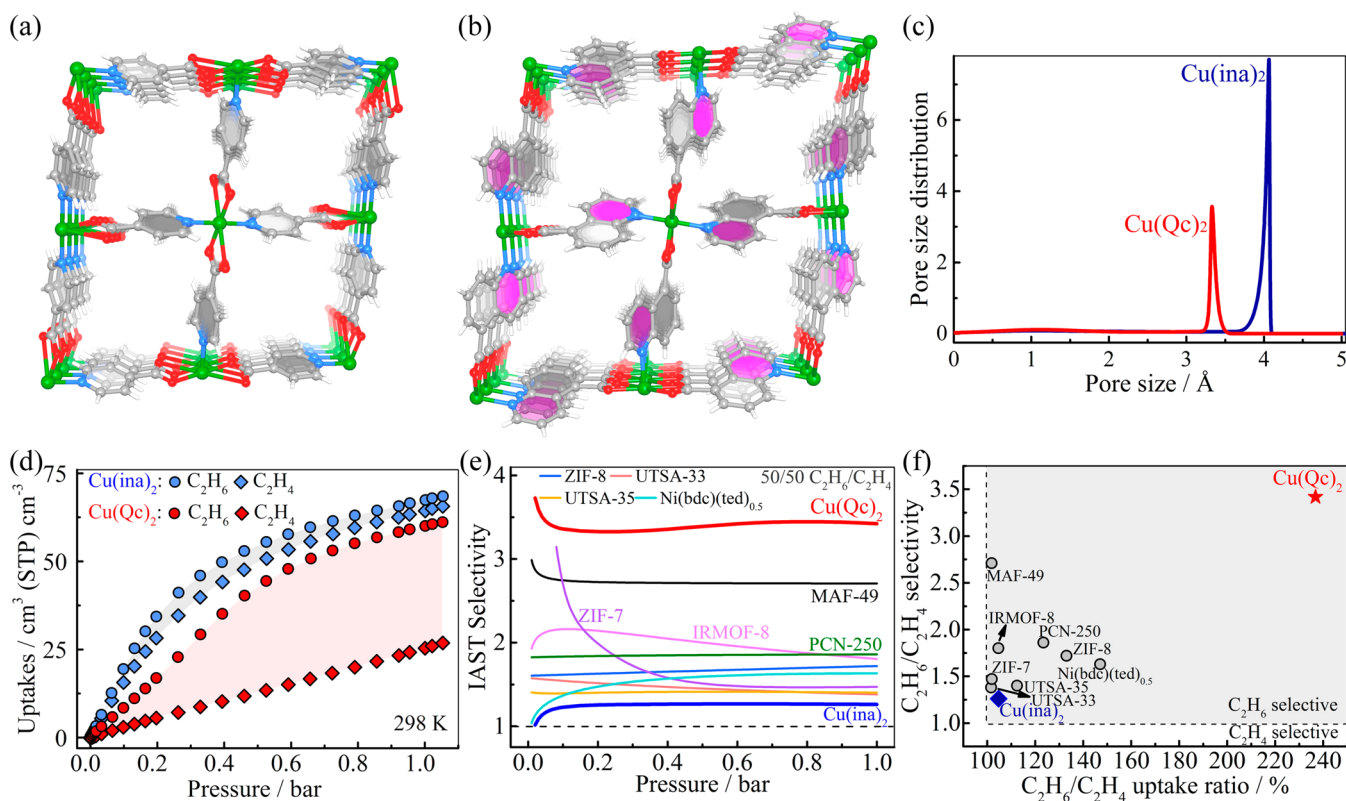


Figure 1. Comparison of crystal structures and channels between $\text{Cu}(\text{ina})_2$ (a) and $\text{Cu}(\text{Qc})_2$ (b); Cu, O, N, and C are represented by green, red, light blue, and gray, respectively, and guest molecules are omitted for clarity. (c) Pore size distribution for $\text{Cu}(\text{ina})_2$ and $\text{Cu}(\text{Qc})_2$, based on sphere probes. (d) C_2H_6 and C_2H_4 sorption isotherms for $\text{Cu}(\text{ina})_2$ and $\text{Cu}(\text{Qc})_2$ at 298 K. (e) Pressure-dependent $\text{C}_2\text{H}_6/\text{C}_2\text{H}_4$ selectivities for $\text{Cu}(\text{ina})_2$ and $\text{Cu}(\text{Qc})_2$ in comparison to the best materials reported to date. (f) $\text{C}_2\text{H}_6/\text{C}_2\text{H}_4$ selectivities/uptake ratios for $\text{Cu}(\text{ina})_2$ (blue diamond) and $\text{Cu}(\text{Qc})_2$ (red star) at 298 K and 1 bar.

only copper quinoline-5-carboxylate ($\text{Cu}(\text{Qc})_2$)¹⁷ was accordingly evaluated with $\text{Cu}(\text{ina})_2$. In both MOFs, each Cu(II) atom is coordinated by two pyridyl/quinoline groups (with two N atoms) and two carboxylate groups (with four O atoms), which is expanded to four adjacent Cu(II) atoms through two-connected ligands, affording square lattice (sql) coordination network (Figure 1a–b). The layered networks further stack together through π – π interactions. As-synthesized samples were prepared under solvothermal conditions, and their phase purity was confirmed through comparing their experimental PXRD patterns with the corresponding simulated ones from single crystal data (Figures S1–2, see Supporting Information). After guest removal from the as-synthesized samples, both structures of $\text{Cu}(\text{ina})_2$ and $\text{Cu}(\text{Qc})_2$ shrink to more dense phases, exhibiting one-dimensional (1D) channels with aperture sizes of ~ 4.1 and ~ 3.3 Å (void space of 22.3% and 17.2%, cavity size of $5.4 \times 5.8 \times 6.3$ and $4.7 \times 6.1 \times 6.6$ Å³), respectively (Figures 1c and S3). The accessible pore surfaces of these two MOFs are mainly occupied by low polarity aromatic rings. Consequently, such ultramicroporous structures are particularly promising for preferential ethane accommodation, considering that their low-polarity pore surfaces are more favorable for ethane molecules of larger polarizability (Table S2).

The Brunauer–Emmett–Teller surface areas of activated $\text{Cu}(\text{ina})_2$ and $\text{Cu}(\text{Qc})_2$ were measured to be 228 and 240 m²/g (Langmuir surface area: 260 and 290 m²/g), respectively, by CO₂ sorption experiment at 195 K (Figure S4). Their total pore volumes were measured to be 0.10 and 0.11 cm³/g, which

is a little lower than the theoretical pore volumes from corresponding crystal structures (0.15 and 0.12 cm³/g), owing to slightly insufficient filling of CO₂ on the undulating pore surfaces.

The inert pore surface and suitable pore size of $\text{Cu}(\text{ina})_2$ and $\text{Cu}(\text{Qc})_2$ provide us the initial motivation to evaluate their C_2H_6 and C_2H_4 sorption performance. Hence, low-pressure C_2H_6 and C_2H_4 sorption data under ambient conditions were collected (Figure 1d). Indeed, $\text{Cu}(\text{ina})_2$ shows ethane-selective sorption behavior, with uptake capacity of 67.4 cm³ cm⁻³ (1.99 mmol g⁻¹) for C_2H_6 and 64.3 cm³ cm⁻³ (1.90 mmol g⁻¹) for C_2H_4 at 298 K and 1 bar, giving a $\text{C}_2\text{H}_6/\text{C}_2\text{H}_4$ uptake ratio of 105%. In contrast, for $\text{Cu}(\text{Qc})_2$, with smaller pore aperture sizes and featuring larger aromatic π systems, more distinct ethane-selective sorption performance can be observed under the same condition (Figure 1d). $\text{Cu}(\text{Qc})_2$ shows uptake capacity of 60.0 cm³ cm⁻³ (1.85 mmol g⁻¹) for C_2H_6 and 25.3 cm³ cm⁻³ (0.78 mmol g⁻¹) for C_2H_4 at 298 K and 1 bar, giving a $\text{C}_2\text{H}_6/\text{C}_2\text{H}_4$ uptake ratio of 237%, which is higher than those of other MOF materials (Table S3).^{15,21} The adsorption of relatively large gas molecules into $\text{Cu}(\text{Qc})_2$ with smaller pore aperture indicates the dynamic nature of such structure. The C_2H_6 uptake capacity of $\text{Cu}(\text{Qc})_2$ is comparable to benchmark MAF-49 (1.73 mmol g⁻¹) and ZIF-7 (1.83 mmol g⁻¹) (Table S3).^{15,21} Notably, according to the amount of adsorbed C_2H_6 in $\text{Cu}(\text{Qc})_2$ and the corresponding pore volume, the density of encapsulated C_2H_6 in the pore channels at 298 K is up to 464 g/L, which is about 380 times as gaseous C_2H_6 density of 1.22 g/L (298 K, 1 bar) and close to the liquid C_2H_6 density of 543

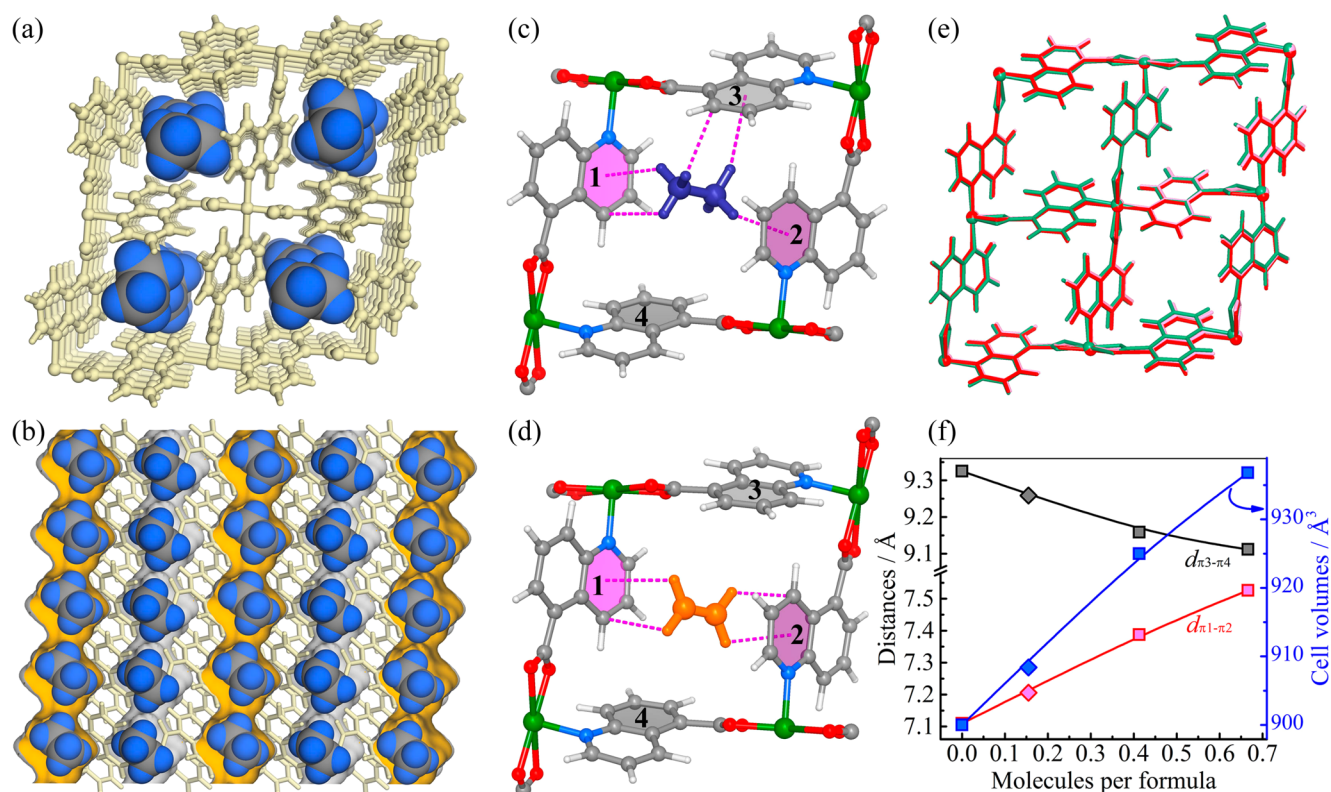


Figure 2. Neutron diffraction crystal structures of $[\text{Cu}(\text{Qc})_2] \cdot 0.41\text{C}_2\text{D}_6$ (a–c) and $[\text{Cu}(\text{Qc})_2] \cdot 0.16\text{C}_2\text{D}_4$ (d); Cu, O, N, and C are represented by green, red, light blue, and gray, respectively. (c and d) Preferential binding sites for C_2D_6 and C_2D_4 molecules and the close vdW contacts within the rhombic cavity of aromatic rings (numbered as 1–4), highlighted C–H... π interactions in pink dashed bonds. (e) Slight structural deformations of the framework in different C_2D_6 -loading structures, bare: sea green, low loading: rose, high loading: red. (f) Ethane-loading dependent evolution of structural parameters, including distances of rings 1 to 2 ($d_{\pi_1-\pi_2}$) and rings 3 to 4 ($d_{\pi_3-\pi_4}$); diamond symbols are for ethylene, and lines are to guide the eye.

g/L (184.6 K, 1.01 bar), implying the highly efficient packing of ethane molecules in $\text{Cu}(\text{Qc})_2$. In fact, the introduction of large substituted organic moieties can reduce the pore volume, resulting in a decrease of gas uptake capacity in the absence of strong adsorption sites. Indeed, the larger quinoline moieties in $\text{Cu}(\text{Qc})_2$ dramatically lowered its uptake capacity for C_2H_4 . Surprisingly, they showed negligible effect on that of C_2H_6 , as indicated by cycling sorption measurements (Figures S5–6). Obviously, the only thing can be foreseen is that strengthened interactions happen between ethane molecules and the framework of $\text{Cu}(\text{Qc})_2$.

To make a quantitative comparison of these different interactions in $\text{Cu}(\text{Qc})_2$, modeling studies based on first-principles dispersion-corrected density functional theory (DFT-D) were conducted. Primarily van der Waals (vdW) interactions can be found after loading of C_2H_6 molecules into the framework of $\text{Cu}(\text{Qc})_2$. The calculated static adsorption energy (ΔE , only involving the host–guest interactions) for C_2H_6 is 37.6 kJ mol^{-1} . In contrast, the ΔE for C_2H_4 is significantly lower and only 23.1 kJ mol^{-1} , which implies a weaker host–guest interaction. Simultaneously, coverage-dependent adsorption enthalpies (Q_{st}) of $\text{Cu}(\text{Qc})_2$ for C_2H_6 and C_2H_4 were evaluated experimentally from pure component isotherms collected at 273, 298, and 313 K, by using the Clausius–Clapeyron equation (Figures S7–8). The resultant Q_{st} for C_2H_6 at near-zero coverage is $29 \pm 2 \text{ kJ mol}^{-1}$, involving the host–guest interactions for C_2H_6 and certain endothermic framework distortions, which certainly is higher

than that of 25.4 kJ mol^{-1} for C_2H_4 . At higher coverage, the adsorption enthalpy for C_2H_6 is maintained on $30\text{--}31 \text{ kJ mol}^{-1}$, while that for C_2H_4 is only $24\text{--}25 \text{ kJ mol}^{-1}$. In addition, the Q_{st} of $\text{Cu}(\text{ina})_2$ for C_2H_6 and C_2H_4 is 26.5 and 25.8 kJ mol^{-1} , respectively (Figures S9–10), which is fully consistent with the variation of their polarizabilities and adsorption uptakes. Obviously, the larger difference of the adsorption enthalpies for C_2H_6 and C_2H_4 can result in the larger $\text{C}_2\text{H}_6/\text{C}_2\text{H}_4$ uptake ratio. Hence, for C_2H_6 and C_2H_4 molecules, their binding affinity from the inert surface relies on the variation of efficient contact area or interactions number, which is very sensitive to the pore structure.

To visualize and structurally understand these host–guest interactions, we carried out high-resolution neutron powder diffraction (NPD) measurements to determine the binding conformations of C_2H_6 and C_2H_4 molecules in $\text{Cu}(\text{Qc})_2$. The loading amounts of both gases were controlled by their backfill pressure. High-quality NPD data of the gas-loaded $\text{Cu}(\text{Qc})_2$ samples were collected at room temperature (Figures S11–12), in which the conformation of gas molecules were successfully identified. As shown in Figure 2, based on the data of $[\text{Cu}(\text{Qc})_2] \cdot 0.41\text{C}_2\text{D}_6$, there is only one crystallographically independent C_2D_6 molecule in the pore systems. Specifically, C_2D_6 molecule locates in a rhombic cavity formed by aromatic rings (mainly refers to rings 1–4 in Figure 2c) of ligands from the same layered network, giving a sandwich structure as viewed along two adjacent rhombic edges. The C_2D_6 occupancy was determined by free structural refinement

to be 0.413(5), which is equivalent to 1 mmol g⁻¹ (sealed at 0.4 bar), as consistent with that from the gas sorption experiment (1.1 mmol g⁻¹). Compared with the bare Cu(Qc)₂, the unit cell of [Cu(Qc)₂]₂·0.41C₂D₆ exhibits certain expansion and slight deformation ($\Delta V/V_{\text{bare}} = 2.9\%$, $\Delta\beta = 0.6^\circ$). As expected, multiple C–D··· π interactions (D··· π 2.34(3)–3.34(3) Å, C–D··· π 3.22(3)–4.16(3) Å) were found between each C₂D₆ molecule and the aromatic rings within the rhombic cavity, most of which are shorter than the sum of the vdW radii of hydrogen/carbon (1.20/1.70 Å) and carbon (1.70 Å) atoms. It should be noted that weakly polar C–H··· π interactions are more like weaker interactions dominated by dispersion, as compared to other intermolecular hydrogen-bond-like interactions (i.e., O–H··· π and N–H··· π), all of which make essential contributions to biomacromolecules structure.²² The interaction energy of a typical C–H··· π interaction is calculated to be only 6.1 kJ mol⁻¹.²³ Nevertheless, the optimized cavity of Cu(Qc)₂ fits well with the molecule shape of C₂H₆, which enables the binding for C₂H₆ through multiple C–H··· π interactions come into reality. It can be identified from the C₂D₆ loaded structure where the ethane molecule with staggered conformation contributes five of its six hydrogen atoms to form C–H··· π interactions.

In contrast, prepared under the same conditions, the structure of [Cu(Qc)₂]₂·0.16C₂D₄ exhibits a negligible structural deformation ($\Delta V/V_{\text{bare}} = 0.9\%$, $\Delta\beta = 0.1^\circ$, see Figure S13). The C₂D₄ occupancy from free refinement is only 0.155(5). The C₂D₄ molecule shows short contacts with only two parallel edges of the rhombic cavity (Figure 2d), giving a similar sandwich structure. Similar clear C–D··· π interactions (D··· π 2.51(12)–2.92(12) Å, C–D··· π 2.94(12)–3.33(12) Å) were also found between each C₂D₄ molecule and the aromatic rings. Obviously, although all four hydrogen atoms of ethylene molecule are involved in the C–H··· π interactions, its lower adsorption heat (~6 kJ mol⁻¹ less than that for C₂H₆) can be attributed to the less involved hydrogen atoms as compared to ethane. Accordingly, for ethane, the more C–H··· π interactions and higher occupancy indicate its higher binding affinity.

To well understand the sorption behaviors, the structure of high C₂D₆-loading sample [Cu(Qc)₂]₂·0.67C₂D₆ was also measured (Figure S14). The same preferential binding site with higher C₂D₆ occupancy of 0.666(6) was determined from this data. Besides, a slightly larger structural deformation ($\Delta V/V_{\text{bare}} = 4.1\%$, $\Delta\beta = 0.9^\circ$) can be observed, showing self-adaptive behavior for different C₂H₆ loadings. The same hydrogen atoms formed multiple C–H··· π interactions (D··· π 2.410(4)–3.186(4) Å, C–D··· π 3.289(4)–4.052(4) Å) with the aromatic rings inside the rhombic cavity, while no noticeable adsorbate–adsorbate interaction can be found. Notably, comparing with the low loading structure, C₂D₆ molecule in [Cu(Qc)₂]₂·0.67C₂D₆ forms closer contacts with the third aromatic ring (Figure 2c, ring 3, D··· π ₃ 2.844(5)–3.186(4) Å, C–D··· π ₃ 3.595(5)–4.052(4) Å), which is consistent with the trend of adsorption enthalpy, and further demonstrates such optimized pore structure is competent to accommodate ethane molecules.

Comparison of the crystal structures with different C₂D₆ loadings further illustrates the self-adaptive adsorption behavior of Cu(Qc)₂ (Figure 2e–f). The framework structure shows continuous swelling and deformation upon the increased loading of C₂H₆, which can be attributed to the close-range repulsion effect (one of contributions to adsorbate–adsorbent interaction potentials,¹³ also the origin

of common steric hindrance effect) as well as the dynamic nature of coordination framework. Interestingly, upon increasing the amount of adsorbed C₂D₆ molecules, the distance between rings 1 and 2 ($d_{\pi_1-\pi_2}$) is swelling, whereas that between rings 3 and 4 ($d_{\pi_3-\pi_4}$) is shrinking owing to the attractions of ethane molecule. Such distinct self-adaptive behavior of the host framework can continuously maintain the close vdW contacts with ethane molecules. On the other hand, the vdW surface area of C₂H₆ (75 Å²) is clearly higher than that of C₂H₄ (61 Å²), which is a prerequisite for larger adsorbate–adsorbent close contact area and/or more corresponding interactions to happen, thus boosting the ethane binding affinity of Cu(Qc)₂.

Motivated by the large C₂H₆/C₂H₄ uptake ratio and preferentially binding of ethane molecules, the selectivity calculation was performed based on the ideal adsorbed solution theory (IAST, Figures S15–24), which can evaluate the potential of Cu(Qc)₂ for ethane removal from the C₂H₄/C₂H₆ mixture. As expected, the calculated C₂H₆/C₂H₄ selectivity of Cu(Qc)₂ for the corresponding binary equimolar mixture is up to 3.4 at 298 K and 100 kPa, which is higher than that for any other top-performing MOF material of ethane selective (Figure 1e–f, Table S3).^{15,21} In contrast, the C₂H₆/C₂H₄ selectivity of Cu(ina)₂ under the same condition is only 1.3, as indicated by its gas isotherms and uptake ratio. Obviously, by virtue of pore engineering to precisely control the pore structure, the resultant MOF material can exhibit not only high uptake ratio but also high selectivity for ethane removal from C₂H₄/C₂H₆ mixture. In addition, activated Cu(Qc)₂ shows remarkable moisture stability under 98% relatively humidity (Figure S25). The results fully support the potential of Cu(Qc)₂ in practical C₂H₆/C₂H₄ separation at ambient pressure.

To further evaluate the C₂H₆/C₂H₄ separation performance of Cu(Qc)₂ in practical adsorption process, we carried out experimental breakthrough studies in which the C₂H₆/C₂H₄ mixture was flowed over a packed column of activated adsorbent with a rate of 2 mL per min at 298 K (see Supporting Information). As shown in Figure 3, complete separation of C₂H₆ from C₂H₆/C₂H₄ mixture can be realized at ambient conditions by using activated Cu(Qc)₂. C₂H₄ can be first detected from the outlet effluent gas during initial purges, showing a desirable purity of over 99.9%, while no detectable C₂H₆ was found. Then, after the adsorbent became saturated

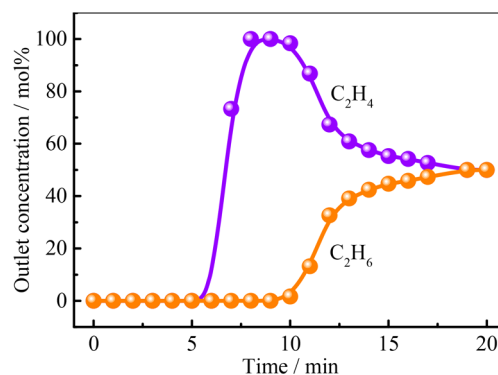


Figure 3. Experimental column breakthrough curves for equimolar C₂H₆/C₂H₄ (orange/purple) mixture (298 K, 1 bar) in an adsorbent bed packed with Cu(Qc)₂.

in the dynamic mixture flow, C_2H_6 reached its breakthrough point, giving a C_2H_4 productivity of 587 mmol/L sorbent. Obviously, by using C_2H_6 -selective adsorbents, the desirable high-purity C_2H_4 can be directly obtained in a single separating operation, which greatly simplifies the separation process of these important petrochemicals.

CONCLUSION

In summary, we report a simple approach to explore ethane-selective MOFs for superior ethane separation technology to advance ethylene production. In principle, the introduction of highly polar binding sites onto the pore surface of MOFs will facilitate their binding affinity for more polar molecules like ethylene, giving ethylene-selective adsorbents. For the much more challenging design of ethane-selective MOFs, strong binding sites are hardly available, whereas increasing the efficient contact area or the quantity of interactions is more applicable. By virtue of pore engineering, we can successfully target an inert ultramicroporous material with optimized pore structure, which realizes highly ethane-selective sorption behavior. The self-adaptive pore structure in this MOF can maximize the quantity and contact area of adsorbate–adsorbent interactions, resulting in larger binding affinity for ethane over ethylene, which is well supported by direct crystallography studies. This approach will facilitate future design and implementation of efficient porous MOF materials for separating important chemicals.

ASSOCIATED CONTENT

Supporting Information

The Supporting Information is available free of charge on the ACS Publications website at DOI: 10.1021/jacs.8b07563.

Crystallographic data, additional structural plot, TG curves, PXRD, multiple cycles sorption isotherms, NPD data for Rietveld refinement, Langmuir–Freundlich isotherm model fitting, isosteric heat of adsorption, IAST calculations of adsorption selectivities, and comparison of ethane-selective MOFs (PDF)

Crystallographic data for $[Cu(Qc)_2] \cdot 0.41C_2D_6$, $[Cu(Qc)_2] \cdot 0.16C_2D_4$, $[Cu(Qc)_2] \cdot 0.67C_2D_6$, and $[Cu(Qc)_2]$ (CIF)

AUTHOR INFORMATION

Corresponding Authors

*wzhou@nist.gov

*banglin.chen@utsa.edu

ORCID

Rui-Biao Lin: 0000-0003-3267-220X

Hui Wu: 0000-0003-0296-5204

Junkuo Gao: 0000-0001-9778-4312

Wei Zhou: 0000-0002-5461-3617

Banglin Chen: 0000-0001-8707-8115

Notes

The authors declare no competing financial interest.

ACKNOWLEDGMENTS

This work was supported by the grant AX-1730 from the Welch Foundation (B.C.), National Natural Science Foundation of China (21576006, L.L.), and Foundation of State Key Laboratory of Coal Conversion (J18-19-610, L.L.).

REFERENCES

- (1) Amghizar, I.; Vandewalle, L. A.; Van Geem, K. M.; Marin, G. B. *Engineering* **2017**, *3*, 171.
- (2) Worrell, E.; Phylipsen, D.; Einstein, D.; Martin, N. *Energy Use and Energy Intensity of the U.S. Chemical Industry*; Energy Analysis Department, Environmental Energy Technologies Division, Ernest Orlando Lawrence Berkeley National Laboratory: Berkeley, CA, 2000.
- (3) Sholl, D. S.; Lively, R. P. *Nature* **2016**, *532*, 435.
- (4) Bereciartua, P. J.; Cantín, Á.; Corma, A.; Jordá, J. L.; Palomino, M.; Rey, F.; Valencia, S.; Corcoran, E. W.; Kortunov, P.; Ravikovitch, P. I.; Burton, A.; Yoon, C.; Wang, Y.; Paur, C.; Guzman, J.; Bishop, A. R.; Casty, G. L. *Science* **2017**, *358*, 1068.
- (5) Aguado, S.; Bergeret, G.; Daniel, C.; Farrusseng, D. *J. Am. Chem. Soc.* **2012**, *134*, 14635.
- (6) (a) Furukawa, H.; Cordova, K. E.; O’Keeffe, M.; Yaghi, O. M. *Science* **2013**, *341*, 1230444. (b) Kitagawa, S. *Angew. Chem., Int. Ed.* **2015**, *54*, 10686. (c) Cui, Y.; Li, B.; He, H.; Zhou, W.; Chen, B.; Qian, G. *Acc. Chem. Res.* **2016**, *49*, 483. (d) Shimizu, G. K. H. *Nat. Energy* **2017**, *2*, 842. (e) Li, P.; Chen, Q.; Wang, T. C.; Vermeulen, N. A.; Mehdi, B. L.; Dohnalkova, A.; Browning, N. D.; Shen, D.; Anderson, R.; Gómez-Gualdrón, D. A.; Cetin, F. M.; Jagiello, J.; Asiri, A. M.; Stoddart, J. F.; Farha, O. K. *Chem. Mater.* **2018**, *4*, 1022. (f) Yuan, S.; Feng, L.; Wang, K.; Pang, J.; Bosch, M.; Lollar, C.; Sun, Y.; Qin, J.; Yang, X.; Zhang, P.; Wang, Q.; Zou, L.; Zhang, Y.; Zhang, L.; Fang, Y.; Li, J.; Zhou, H.-C. *Adv. Mater.* **2018**, *30*, 1704303.
- (7) (a) Zhao, X.; Wang, Y.; Li, D.-S.; Bu, X.; Feng, P. *Adv. Mater.* **2018**, *30*, 1705189. (b) Mukherjee, S.; Desai, A. V.; Ghosh, S. K. *Coord. Chem. Rev.* **2018**, *367*, 82. (c) Wang, H.; Zhu, Q.-L.; Zou, R.; Xu, Q. *Chem.* **2017**, *2*, 52. (d) Wang, S.; Kitao, T.; Guillou, N.; Wahiduzzaman, M.; Martineau-Corcoc, C.; Nouar, F.; Tissot, A.; Binet, L.; Ramsahye, N.; Devautour-Vinot, S.; Kitagawa, S.; Seki, S.; Tsutsui, Y.; Briois, V.; Steunou, N.; Maurin, G.; Uemura, T.; Serre, C. *Nat. Commun.* **2018**, *9*, 1660. (e) Hendon, C. H.; Rieth, A. J.; Korzyński, M. D.; Dincă, M. *ACS Cent. Sci.* **2017**, *3*, 554. (f) Lan, G.; Ni, K.; Lin, W. *Coord. Chem. Rev.* **2017**, DOI: 10.1016/j.ccr.2017.09.007.
- (8) (a) Adil, K.; Belmabkhout, Y.; Pillai, R. S.; Cadiau, A.; Bhatt, P. M.; Assen, A. H.; Maurin, G.; Eddaoudi, M. *Chem. Soc. Rev.* **2017**, *46*, 3402. (b) Bao, Z.; Chang, G.; Xing, H.; Krishna, R.; Ren, Q.; Chen, B. *Energy Environ. Sci.* **2016**, *9*, 3612. (c) Liao, P.-Q.; Huang, N.-Y.; Zhang, W.-X.; Zhang, J.-P.; Chen, X.-M. *Science* **2017**, *356*, 1193.
- (9) (a) Bloch, E. D.; Queen, W. L.; Krishna, R.; Zdrozny, J. M.; Brown, C. M.; Long, J. R. *Science* **2012**, *335*, 1606. (b) Yang, S.; Ramirez-Cuesta, A. J.; Newby, R.; Garcia-Sakai, V.; Manuel, P.; Callear, S. K.; Campbell, S. I.; Tang, C. C.; Schröder, M. *Nat. Chem.* **2015**, *7*, 121. (c) Sen, S.; Hosono, N.; Zheng, J.-J.; Kusaka, S.; Matsuda, R.; Sakaki, S.; Kitagawa, S. *J. Am. Chem. Soc.* **2017**, *139*, 18313.
- (10) (a) Cui, X.; Chen, K.; Xing, H.; Yang, Q.; Krishna, R.; Bao, Z.; Wu, H.; Zhou, W.; Dong, X.; Han, Y.; Li, B.; Ren, Q.; Zaworotko, M. J.; Chen, B. *Science* **2016**, *353*, 141. (b) Li, B.; Cui, X.; O’Nolan, D.; Wen, H.-M.; Jiang, M.; Krishna, R.; Wu, H.; Lin, R.-B.; Chen, Y.-S.; Yuan, D.; Xing, H.; Zhou, W.; Ren, Q.; Qian, G.; Zaworotko, M. J.; Chen, B. *Adv. Mater.* **2017**, *29*, 1704210. (c) Lin, R.-B.; Li, L.; Wu, H.; Arman, H.; Li, B.; Lin, R.-G.; Zhou, W.; Chen, B. *J. Am. Chem. Soc.* **2017**, *139*, 8022.
- (11) (a) Li, K.; Olson, D. H.; Seidel, J.; Emge, T. J.; Gong, H.; Zeng, H.; Li, J. *J. Am. Chem. Soc.* **2009**, *131*, 10368. (b) Cadiau, A.; Adil, K.; Bhatt, P. M.; Belmabkhout, Y.; Eddaoudi, M. *Science* **2016**, *353*, 137. (c) Bachman, J. E.; Kapelewski, M. T.; Reed, D. A.; Gonzalez, M. I.; Long, J. R. *J. Am. Chem. Soc.* **2017**, *139*, 15363.
- (12) (a) Li, L.; Lin, R.-B.; Krishna, R.; Wang, X.; Li, B.; Wu, H.; Li, J.; Zhou, W.; Chen, B. *J. Am. Chem. Soc.* **2017**, *139*, 7733. (b) Yang, L.; Cui, X.; Yang, Q.; Qian, S.; Wu, H.; Bao, Z.; Zhang, Z.; Ren, Q.; Zhou, W.; Chen, B.; Xing, H. *Adv. Mater.* **2018**, *30*, 1705374.
- (13) Yang, R. T. *Adsorbents: Fundamentals and Applications*; John Wiley & Sons, Inc.: Hoboken, NJ, 2003.
- (14) Li, J.-R.; Kuppler, R. J.; Zhou, H.-C. *Chem. Soc. Rev.* **2009**, *38*, 1477.

(15) (a) Liao, P.-Q.; Zhang, W.-X.; Zhang, J.-P.; Chen, X.-M. *Nat. Commun.* **2015**, *6*, 8697. (b) Gücüyener, C.; van den Bergh, J.; Gascon, J.; Kapteijn, F. *J. Am. Chem. Soc.* **2010**, *132*, 17704.

(16) Li, B.; Zhang, Y.; Krishna, R.; Yao, K.; Han, Y.; Wu, Z.; Ma, D.; Shi, Z.; Pham, T.; Space, B.; Liu, J.; Thallapally, P. K.; Liu, J.; Chrzanowski, M.; Ma, S. *J. Am. Chem. Soc.* **2014**, *136*, 8654.

(17) Chen, K.-J.; Madden, D. G.; Pham, T.; Forrest, K. A.; Kumar, A.; Yang, Q.-Y.; Xue, W.; Space, B.; Perry, J. J.; Zhang, J.-P.; Chen, X.-M.; Zaworotko, M. *Angew. Chem., Int. Ed.* **2016**, *55*, 10268.

(18) Lu, J. Y.; Babb, A. M. *Chem. Commun.* **2003**, 1346.

(19) Larson, A. C.; Von Dreele, R. B. *General Structure Analysis System*, Report LAUR 86-748; Los Alamos National Laboratory: Los Alamos, NM, 1994.

(20) Bu, X.-H.; Tong, M.-L.; Xie, Y.-B.; Li, J.-R.; Chang, H.-C.; Kitagawa, S.; Ribas, J. *Inorg. Chem.* **2005**, *44*, 9837.

(21) (a) Liang, W.; Xu, F.; Zhou, X.; Xiao, J.; Xia, Q.; Li, Y.; Li, Z. *Chem. Eng. Sci.* **2016**, *148*, 275. (b) Chen, Y.; Qiao, Z.; Wu, H.; Lv, D.; Shi, R.; Xia, Q.; Zhou, J.; Li, Z. *Chem. Eng. Sci.* **2018**, *175*, 110.

(22) Plevin, M. J.; Bryce, D. L.; Boisbouvier, J. *Nat. Chem.* **2010**, *2*, 466.

(23) Tsuzuki, S.; Honda, K.; Uchimaru, T.; Mikami, M.; Tanabe, K. *J. Am. Chem. Soc.* **2000**, *122*, 11450.